Supplementary Information for

Conductive RuO_2 Binders Enhance Mechanical Stability of Macroporous Nb-SnO_2 Particles as Cathode Catalyst Supports for High-Performance PEFCs

Thi Thanh Nguyen Ho[1], Tomoyuki Hirano[1], Aoi Takano[2], Syu Miyasaka[2], Eishi Tanabe[3], Makoto Maeda[4], Eka Lutfi Septiani[1], Kiet Le Anh Cao[1] and Takashi Ogi[1*]*

[1]Chemical Engineering Program, Graduate School of Advanced Science and Engineering, Hiroshima University, 1–4–1 Kagamiyama, Higashihiroshima, Hiroshima 739–8527, Japan

[2]Cataler Corporation, 7800 Chihama, Kakegawa, Shizuoka 437-1492, Japan

[3]Hiroshima Prefectural Institute of Industrial Science and Technology, 3-10-31 Kagamiyama, Higashi Hiroshima, Hiroshima 739-0046, Japan

[4]Natural Science Center for Basic Research and Development, Hiroshima University, 1–4–1 Kagamiyama, Higashihiroshima, Hiroshima 739–8527, Japan

*Corresponding Author:

Tomoyuki Hirano; Email: tomoyuki-hirano@hiroshima-u.ac.jp; Phone: +81-82-424-7850

Takashi Ogi; Email: ogit@hiroshima-u.ac.jp; Phone: +81-82-424-3765

KEYWORDS: macroporous structure, mechanical stability, polymer electrolyte fuel cells, ruthenium oxide, binder, flame aerosol, nanostructured particle.

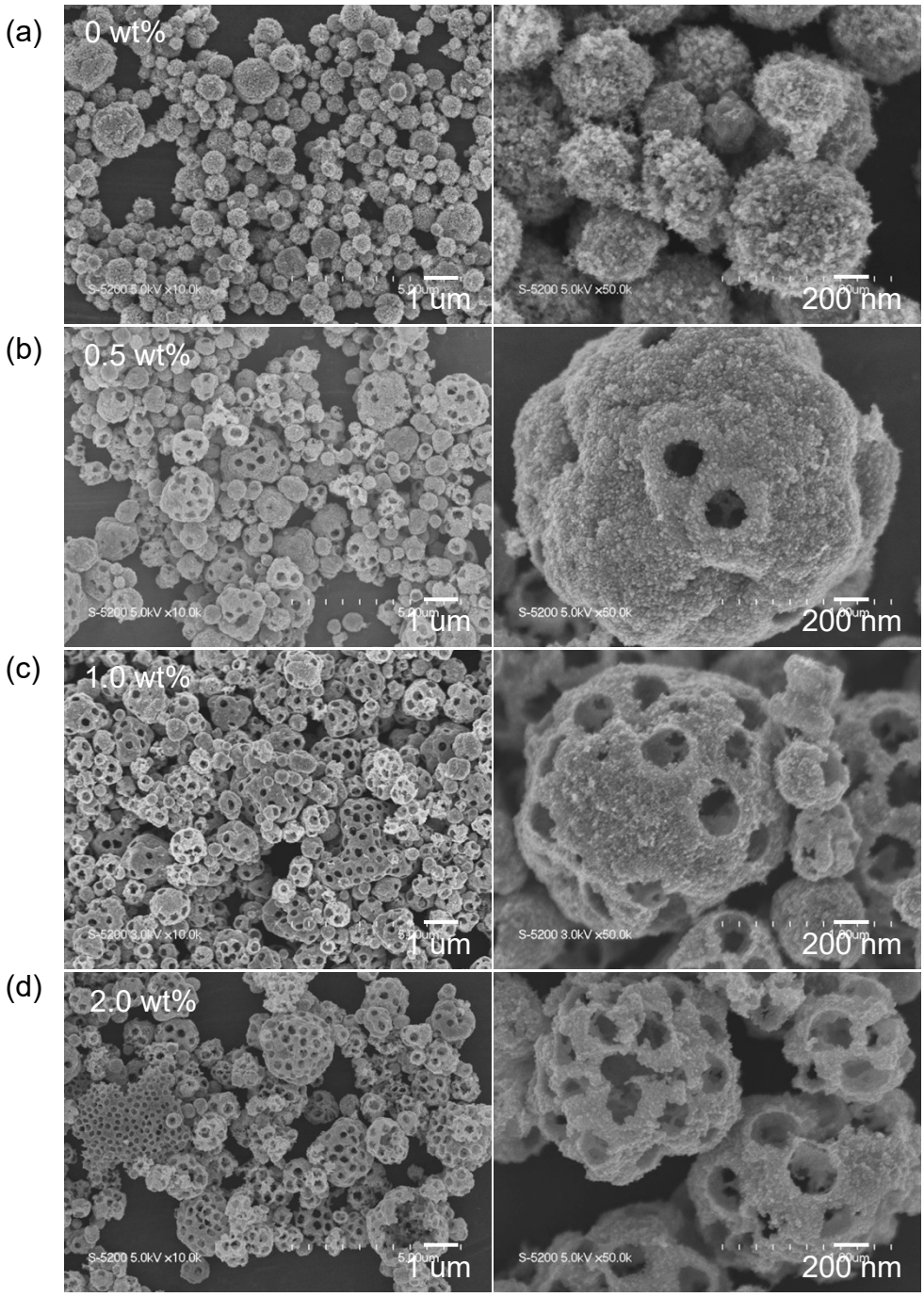

Figure S1. SEM images of macroporous NTO/RuO_2–50 particles with different PMMA concentrations: (a) 0 wt.%, (b) 0.5 wt.%, (c) 1.0 wt.%, and (d) 2.0 wt.%.

We systematically investigated the effect of PMMA template concentration on the macroporous structure of NTO/RuO_2 particles by employing a constant RuO_2 binder concentration of 50 wt%. The morphological changes induced by different PMMA concentrations were characterized using SEM. In the absence of a PMMA template, the NTO/RuO_2 particles formed spherical structures of various sizes through aggregation. This phenomenon was attributed to the presence of only $RuCl_3$ and NTO nanoparticles in the precursor droplets, where NTO nanoparticles self-assembled into spherical shapes to minimize free energy, with the RuO_2 binder precipitating between the NTO nanoparticles. Upon the introduction of the 0.5 wt.% PMMA templates, a well-defined macroporous framework was observed, as illustrated in **Figure S1b**. When the PMMA template content was increased to 1.0 wt.%, the macroporous framework was preserved, and the number of open macropores on the particle surfaces increased, as shown in **Figure S1c–d**. The increase in the number of open macropores could enhance mass transport within the reaction environment, thereby improving the performance of PEFCs. However, a further increase in the PMMA concentration resulted in more particles with disrupted frameworks because the formation of additional open macropores led to a reduction in the thickness of the macroporous framework, causing structural instability and eventual collapse. Notably, the morphology of the final product is strongly influenced by the PMMA concentration within the precursor droplets. Although increasing the PMMA concentration in the precursor droplets increased the number of macropores in the final product, excessively high PMMA template concentrations diminished the thickness of the framework, making it too fragile to maintain the spherical morphology of the macroporous particles.

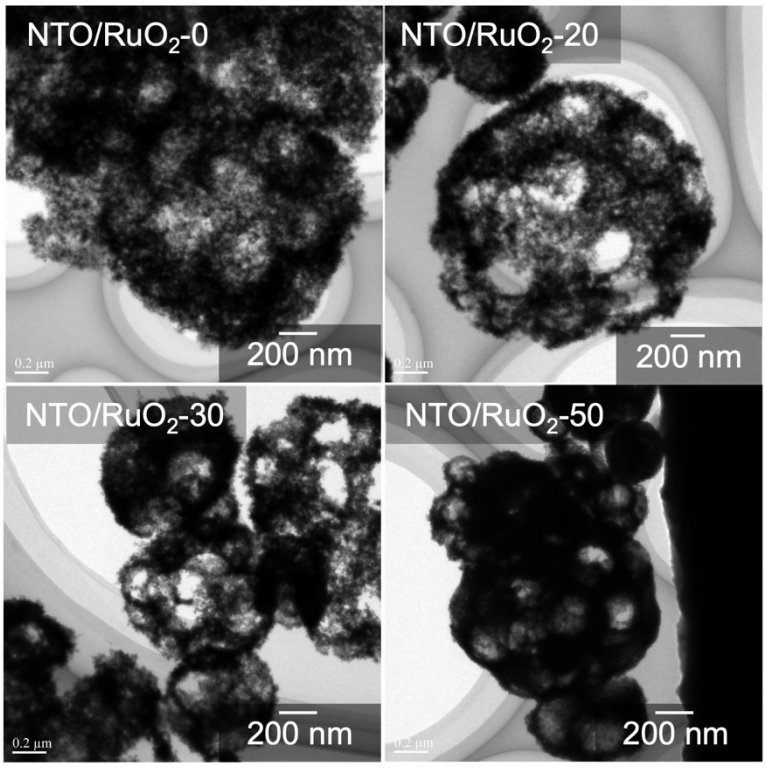

Figure S2. STEM images of macroporous NTO/ RuO_2 particles synthesized with different concentrations of RuO_2 binder.

Table S1. BET surface area measurements

Sample	*S_{BET} (m^2/g)
NTO nanoparticles	106.9
NTO/RuO_2–20	71.1
NTO/RuO_2–20	38.9
NTO/RuO_2–30	38.1
NTO/RuO_2–50	30.4

* Calculated using the BET equation.

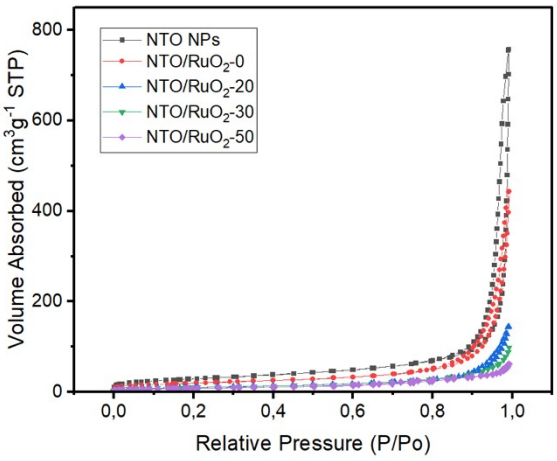

Figure S3. BET nitrogen adsorption isotherm plots of NTO nanoparticles and macroporous NTO/RuO_2 particles.

Table S2. Fractional coordinates and occupancies for macroporous NTO/RuO_2 particles synthesized with different RuO_2 binder contents.

								R_{exp} (%)	R_{wp} (%)	R_p (%)	Crytal size (nm)
			Site	**x**	**y**	**z**	**Occ**				
NTO/RuO_2−20	SnO_2	Sn	2	0	0	0	1	2.88	6.73	5.47	17.9
		O	4	0.305	0.305	0.305	1				
	RuO_2	Ru	2	0	0	0	1				9.31
		O	4	0.305	0.305	0	1				
	Ru metallic	Ru	2p	0.333	0.667	0.250	1				17.3
NTO/RuO_2−30	SnO_2	Sn	2	0	0	0	1	2.90	7.47	5.92	23.0
		O	4	0.305	0.305	0.305	1				
	RuO_2	Ru	2	0	0	0	1				20.3
		O	4	0.305	0.305	0	1				
	Ru metallic	Ru	2p	0.333	0.667	0.250	1				48.4
NTO/RuO_2−50	SnO_2	Sn	2	0	0	0	1	2.74	6.20	4.86	19.9
		O	4	0.305	0.305	0.305	1				
	RuO_2	Ru	2	0	0	0	1				23.0
		O	4	0.305	0.305	0	1				
	Ru metallic	Ru	2p	0.333	0.667	0.250	1				46.7

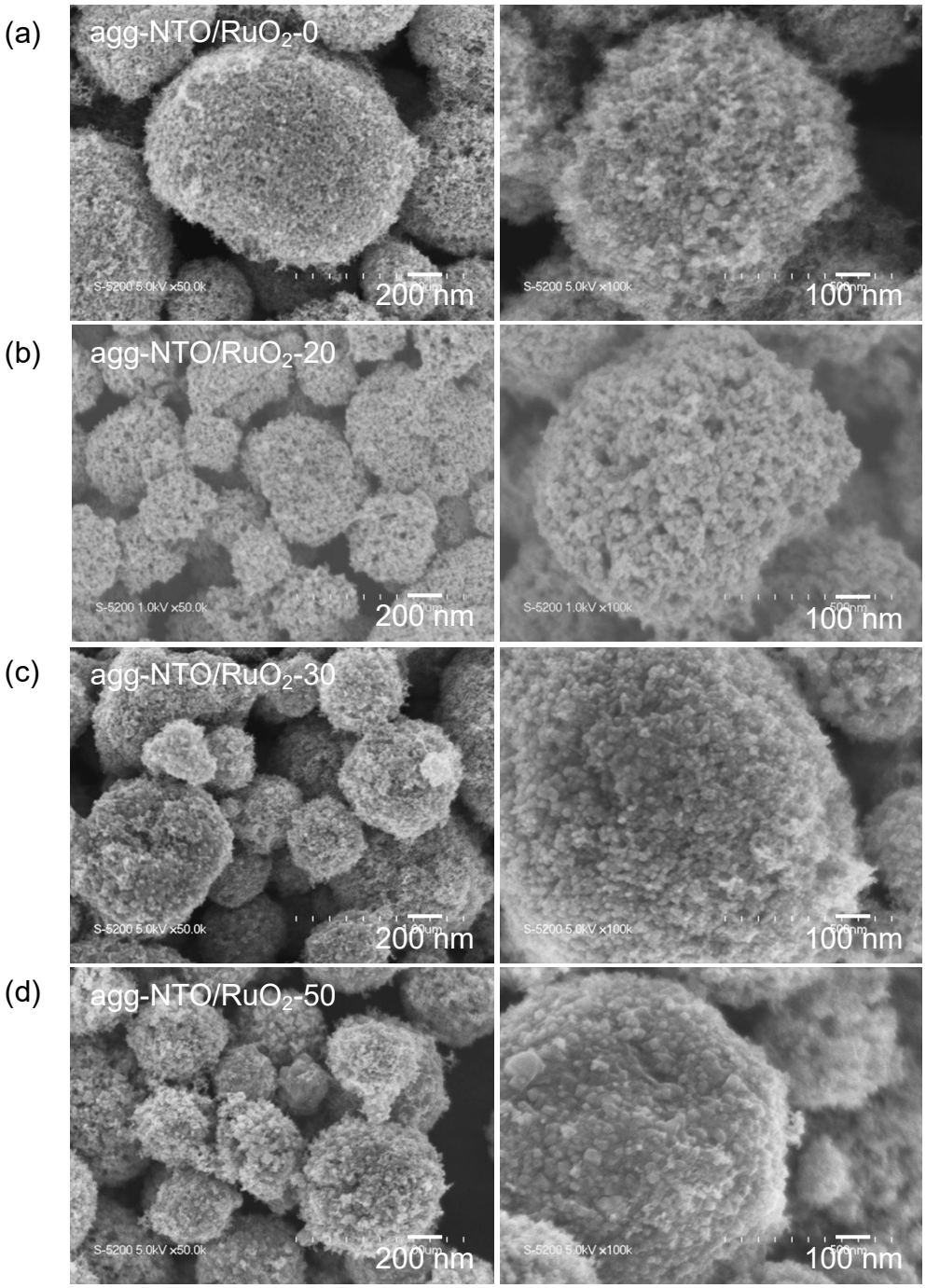

Figure S4. SEM images of aggregated NTO/RuO_2 particles with different RuO_2 binder contents: (a) agg-NTO/RuO_2−0, (b) agg-NTO/RuO_2−20, (c) agg-NTO/RuO_2−30, and (d) agg-NTO/RuO_2−50 particles.

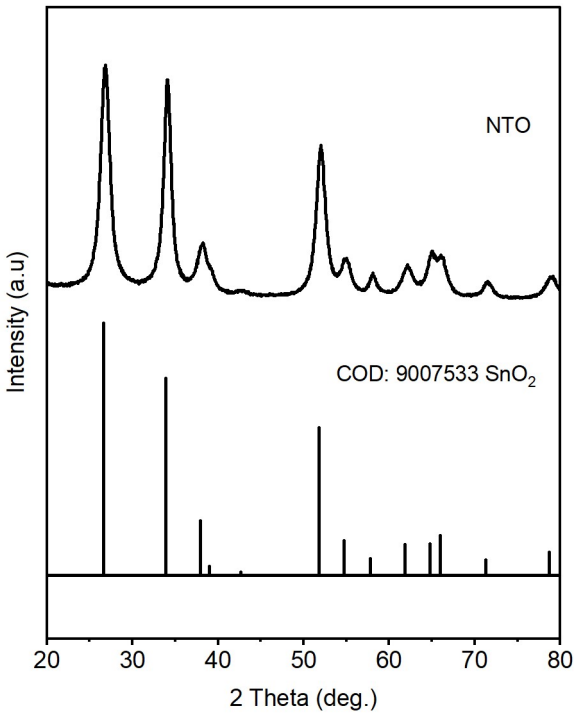

Figure S5. XRD patterns of NTO nanoparticles.

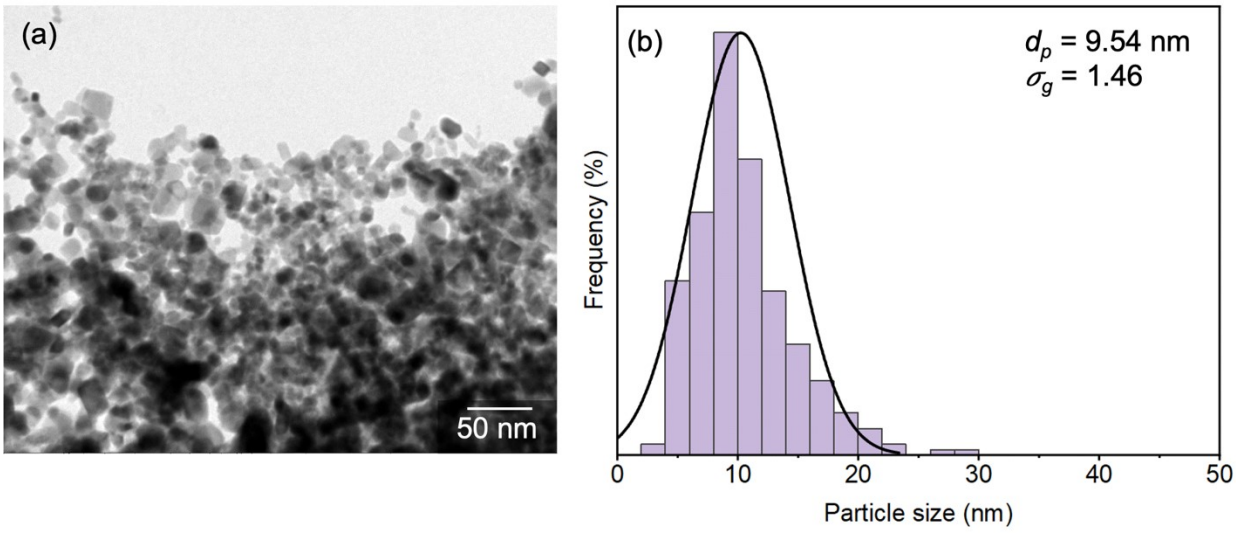

Figure S6. (a)TEM image and (b) size distribution chart of NTO nanoparticles.

In our previous study, we successfully used NTO nanoparticles to prepare macroporous NTO/RuO_2 particles. NTO nanoparticles were synthesized using FSP, and their structural characteristics were analyzed using X–ray diffraction. The XRD patterns reveal that the NTO nanoparticles have a tetragonal SnO_2 structure, as illustrated in **Figure S5**. No discernible diffraction peaks corresponding to Nb are observed. The crystallite size of the NTO nanoparticles was determined to be approximately 9.95 nm using the Scherrer equation. The size distribution of these NTO nanoparticles was assessed based on TEM image analysis using the ImageJ software, and the resulting histogram of the size distribution is presented in **Figure S6**. The average nanoparticle size, as determined from TEM analysis, was 9.54 nm. A slight disparity in crystallite size was observed between the XRD and TEM analyses. This variance can be attributed to the unique necking structure inherent to the NTO nanoparticles synthesized via FSP. These NTO nanoparticles served as precursors for the synthesis of macroporous NTO/RuO_2 particles.

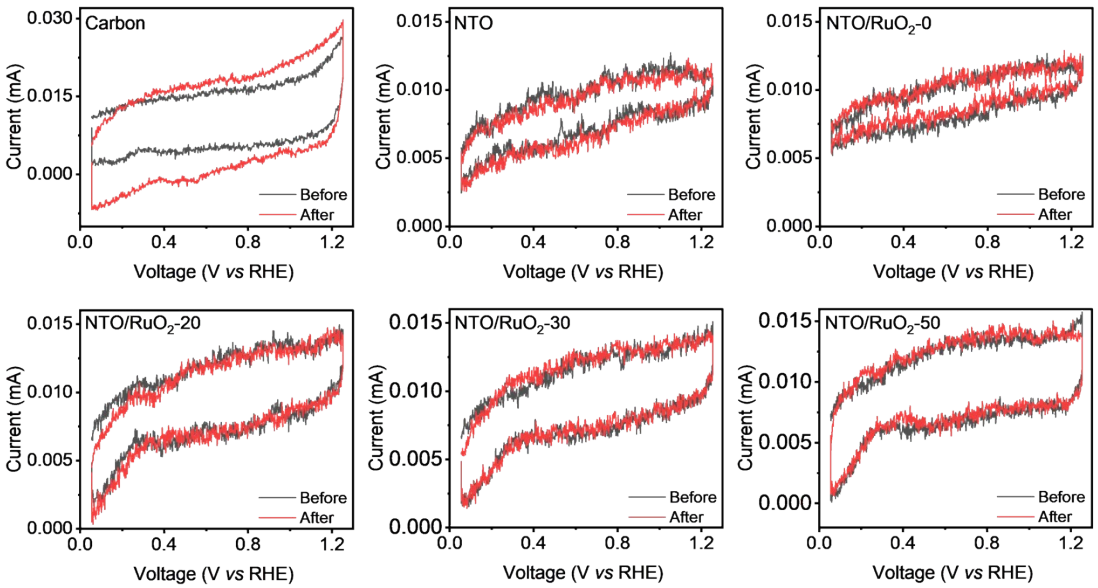

Figure S7. Cyclic voltammograms of carbon, NTO nanoparticles, and macroporous NTO/RuO_2 particles with varying RuO_2 binder contents before and after applying a potential of 1.3 V vs Ag/AgCl for 10 minutes.